J. Biophotonics **5**, No. 5–6, 425–436 (2012) / **DOI** 10.1002/jbio.201100139

Journal of BIOPHOTONICS

FULL ARTICLE

Eliminating the scattering ambiguity in multifocal, multimodal, multiphoton imaging systems

Erich E. Hoover[*,1], *Jeffrey J. Field*[1], *David G. Winters*[2], *Michael D. Young*[1], *Eric V. Chandler*[1], *John C. Speirs*[1], *Jacob T. Lapenna*[1], *Susy M. Kim*[3], *Shi-you Ding*[4], *Randy A. Bartels*[2], *Jing W. Wang*[3], *and Jeff A. Squier*[*,1]

[1] Center for Microintegrated Optics for Advanced Bioimaging and Control, and Department of Physics, Colorado School of Mines, 1523 Illinois Street, Golden, Colorado 80401, USA
[2] Department of Electrical and Computer Engineering, Colorado State University, Fort Collins, Colorado 80523, USA
[3] Section for Neurobiology, Division of Biological Sciences, University of California-San Diego, 9500 Gilman Drive, MC 0368, La Jolla, CA 92093-0368, USA
[4] National Renewable Energy Laboratory, 1617 Cole Boulevard, Golden, Colorado 80401, USA

Received 21 December 2011, revised 1 March 2012, accepted 2 March 2012
Published online 27 March 2012

Key words: multiphoton, multifocal, multimodal, photon counting

In this work we present how to entirely remove the scattering ambiguity present in existing multiphoton multifocal systems. This is achieved through the development and implementation of single-element detection systems that incorporate high-speed photon-counting electronics. These systems can be used to image entire volumes in the time it takes to perform a single transverse scan (four depths simultaneously at a rate of 30 Hz). In addition, this capability is further exploited to accomplish single-element detection of multiple modalities (two photon excited fluorescence and second harmonic generation) and to perform efficient image deconvolution. Finally, we demonstrate a new system that promises to significantly simplify this promising technology.

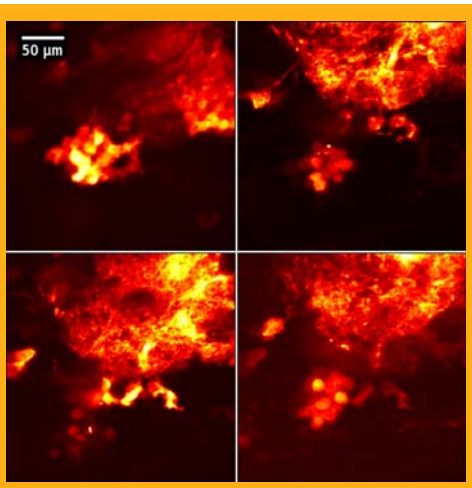

Four images of *Drosophila melanogaster* antennal lobe structure labeled with red fluorescent protein. The images are separated axially by 7 µm in depth and were all acquired simultaneously from a single-element detector.

1. Introduction

The first demonstration of a real-time, video-rate multiphoton microscope was performed with a system that extended the single focal point excitation source to a line cursor geometry [1]. This design incorporated an elegant bilateral scanning system that was used to effectively discriminate against scatter-

* Corresponding authors: e-mail: ehoover@mines.edu, jsquier@mines.edu

ing in one dimension – the direction orthogonal to the line or slit length. With the line cursor geometry, rapid imaging rates are readily achieved. In such a system the line sweeps out a two-dimensional field in the focal plane with a single axis scan, and the multiphoton signal is simultaneously mapped to a two-dimensional detector, such as a charge-coupled-device (CCD) camera.

However, it is worth noting that by moving to a line cursor geometry the image resolution is compromised. In this configuration the beam now features both a high numerical aperture (NA) and a low NA component. The high NA dimension maintains tight lateral resolution, and the low NA dimension determines the axial (or z-axis) resolution. Consequently, the sectioning is, in general, lower for a line cursor as opposed to a point focus.

In order to address this reduction in axial resolution, while maintaining high frame rates, multifocal multiphoton systems were developed. In this geometry, multiple diffraction limited focal spots are created through a variety of mechanisms. Microlens arrays were among the very first devices used to split the ultrafast laser into a large number of diffraction-limited focal spots. This array of foci is then rapidly scanned and the multiphoton signal simultaneously mapped to a two-dimensional detector [2–8]. The basic strategy to bolster high frame rates was to pack the focal plane with as many focal spots as could be reasonably achieved for a given laser source (i.e., produce the maximum number of foci permitted by the available laser power). What became immediately apparent, however, was that as the density of focal spots increased, the axial resolution degraded. In such a situation the focal spots interfere and the effective NA is lowered. Fortunately, when dealing with multiphoton imaging, there is an additional design degree of freedom available that can be used to address this issue: the laser pulse-width. If the individual focal spots are delayed in time by several times their pulse duration, then they cannot interfere and the resolution achieved with a field of focal spots is then identical to that of a single diffraction-limited laser focus [4, 6].

While the resolution issue has been effectively addressed, the utility of multifocal systems has primarily only been exploited in thin, relatively non-scattering specimens. Since two-dimensional detectors must be incorporated, scattered signal light contributes to background and inhibits imaging deeply or within highly scattering media. These scattered photons are the source of the ambiguity, as signal location on a two-dimensional detector does not necessarily correspond to the conjugate position on the specimen. Several effective solutions have now been demonstrated for mitigating the scattering issue when using multifocal imaging systems. For example, by descanning the multiphoton signal, one can significantly extend the depth for which images with a reasonable signal-to-noise ratio can be collected [8, 9]. Our approach to addressing this issue has been to increase the time-delay between foci from picoseconds to nanoseconds and move from integrated detection to photon counting. The implication of this paradigm shift is that, for the first time, the scattering ambiguity is entirely eliminated for multifocal systems.

This approach has enabled multiple focal planes to be imaged in a parallel process; and, hence, entire volumes can now be captured in the time of a single transverse scan. Figure 1 is an example of an image volume captured in this manner. This image displays four different focal planes separated in depth by seven micrometers, all captured simultaneously. In this case, the signal is two-photon excited fluorescence (TPEF) from the antennal lobe of a fruit fly (*Drosophila melanogaster*) genetically engineered to express a red fluorescent protein (mtdTomato) in the projection neurons. Multiple glomeruli and cell bodies found in this structure can be monitored and sampled simultaneously on four different planes. Notably, the image contours presented in all images are not arbitrary units – they are given in actual photon counts.

The utility of this imaging method has recently been further verified by Cheng et al., who used this type of multifocal approach to measure neuronal activity from multiple focal planes inside a living mouse brain by recording TPEF from probes sensitive to calcium activity [10].

To date we have been able to image up to six focal planes, in multiple modalities (e.g., second and third harmonic generation imaging, along with TPEF) simultaneously [11]. In addition, we have added remote focusing capability to the individual planes, providing real-time repositioning of individual focal plane depths [12]. The remote focusing can be used synchronously with the x–y scanners, enabling the focal plane to be rotated or tilted to facilitate more selective viewing of features of interest. In this work, we describe a number of new advancements that further push the capabilities of this new imaging technology. We demonstrate for the first time:

1. a video-rate, photon-counting, multimodal, multifocal imaging system that includes remote focusing;
2. simultaneous image capture using single element detection of multiple modalities without the need for selective spectral filters;
3. the application of programmable gratings for multiphoton image deconvolution;
4. a multimodal, multiphoton line cursor excitation system that only requires single element detection.

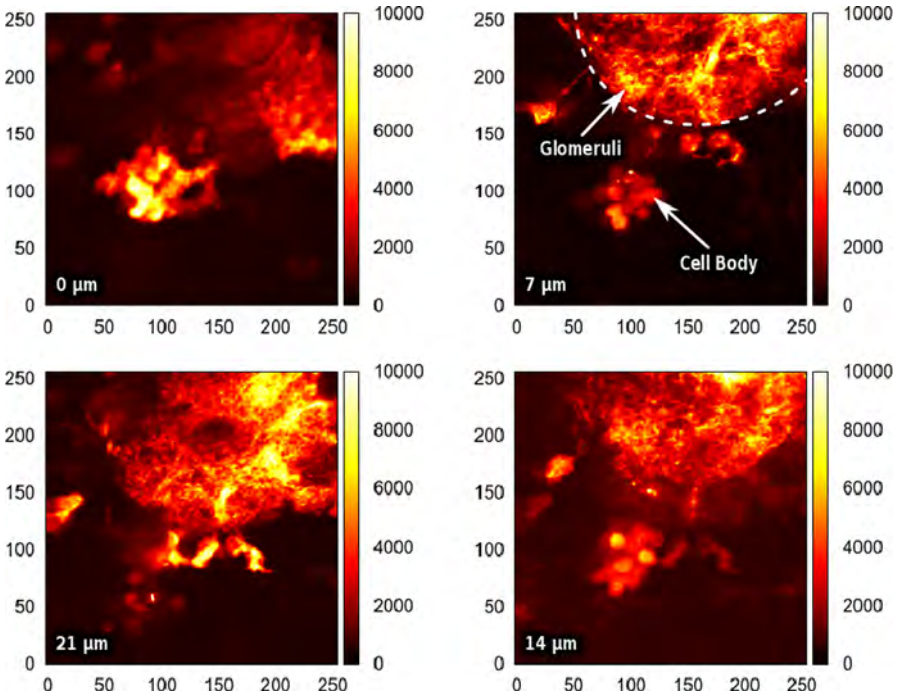

Figure 1 (online color at: www.biophotonics-journal.org) Four images of *Drosophila melanogaster* antennal lobe, where the red fluorescent protein (mtdTomato) has been targeted to projection neurons. The images are separated axially by 7 µm in depth and were all acquired simultaneously. It is of interest to note that different glomeruli and cell bodies, found on different planes, may be sampled simultaneously with this approach. The field of view is 250 by 250 µm, and the number of photon counts (which determine the intensity contours) is denoted on the right hand side of each image by the scale bar. The excitation NA was 0.65, and the excitation wavelength was 1030 nm from a Yb:KGW laser.

2. Video-rate multifocal multimodal photon counting imaging

2.1 Experimental setup

In our most recent work, we demonstrated that remote focusing [13] could be combined with our multifocal, photon counting imaging system [12] to enable simultaneous imaging at multiple depths in scattering specimens. The remote focusing capability makes it possible to select, in real time, variable depths of feature interest. Further, by synchronizing the x or y scanners with the remote focus, the focal plane can be rotated. We demonstrated this capability by capturing image planes rotated 90 degrees with respect to the lateral focus. In this system, the x–y scanning was achieved through a pair of galvanometric scanners. This scan system limited the frame rate capability of the microscope, which was typically operated at pixel dwell times on the order of 10 µs [14]. Here we demonstrate a new scan system that pushes the pixel dwell time down by a factor of 50 and results in true video-rate imaging, allowing us to capture four depths simultaneously at frame rates of 30 Hz. To our knowledge this is the first demonstration of a multimodal, multifocal, photon-counting, video-rate microscope with remote focusing capability.

The improved frame rate was achieved by utilizing a polygonal mirror in place of the traditional fast-axis galvanometric scan mirror [15], as shown in the system schematic in Figure 2. For this work we have implemented the scan system using a Lincoln Laser MC-5 polygonal mirror and a GSI Group, Inc. SC2000 scan mirror. A HeNe laser is reflected off the polygonal mirror and focused onto a photodiode to provide an electronic signal for synchronizing the fast and slow scan axes. An Arduino microcontroller is used to control the polygonal mirror rotation frequency to maintain phase-locked movement with the galvanometric scan mirror. Images are constructed by electronically demultiplexing the photons detected by a Hamamatsu R7400U using the same photon counting method discussed in our previous work [12].

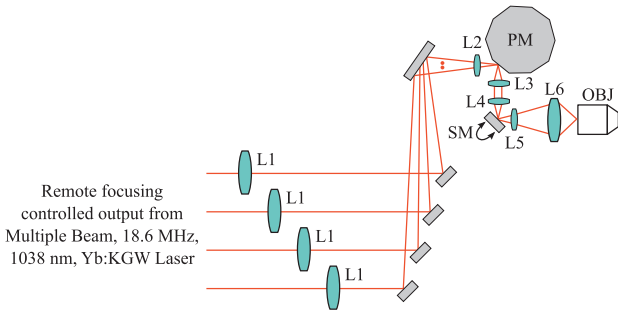

Figure 2 (online color at: www.biophotonics-journal.org) Four beam video-rate imaging system layout. L1: 400 mm Lens, L2: 100 mm Lens, L3: 40 mm Lens, L4: 40 mm Lens, L5: 35 mm Lens, L6: 200 mm Lens, SM: Scan Mirror, PM: Polygonal Mirror, OBJ: Objective.

A significant challenge in constructing a rapid imaging system is implementing electronics that can communicate all of the collected data back to a computer in a timely fashion. To address this issue we transitioned our hardware platform from an Altera DE2 board to an Altera DE3 system, providing us with access to USB 2.0 data-rates. In our previous work all of our data was collected using LabVIEW™ and then rendered using either MATLAB® or gnuplot. Due to the significant overhead incurred when processing data using LabVIEW™, we migrated our data collection over to the open-source μManager software [16]. By transitioning to the DE3 platform and by writing a custom data collection plugin for μManager *we were then able to improve our data-rate from ∼1 MiB/s to ∼20 MiB/s* (a frame rate of 320 Hz for 8-bit 256×256 images). This migration also gave us the ability to have integrated real-time rendering provided by ImageJ, dramatically improving the usability of the system for live data collection.

2.2 Imaging results

Images were collected utilizing a 0.2 microsecond pixel dwell time in order to facilitate video-rate imaging at 30 Hz. This dwell time corresponds to a maximum possible signal of ∼4 counts per pixel per beam for our 18.6 MHz repetition rate. Data corresponding to each of our individual four beams was collected simultaneously as 256×256 4-bit images, resulting in a total acquisition of a 256×1024 frame at 30 Hz (requiring a sustained data rate of 3.75 MiB/s). The resulting image (Figure 3) represents a summation of 900 individual frames (corresponding to 30 seconds of data collection). For these experiments a laser with an excitation wavelength of 1038 nm is used with an average power of 50 mW per beam, as measured at the input of the microscope. The NA of both the excitation and collection objectives is 0.65. For this test, second harmonic generation (SHG) is detected from corn starch granules. The four beams are offset axially with respect to one another by 7 μm, resulting in diminished signal as a function of depth through this thin test sample.

3. Simultaneous single-element multimodal detection

3.1 Experimental setup

We have recently demonstrated that photon-counting imaging is an effective method for measuring fluorescence lifetimes [17]. With the improved data rates provided by the system described in this work, we can push this one step further. We now have the capability to measure fluorescence lifetimes simultaneously from multiple beams; and, as demonstrated in the following images, the ability to discriminate between harmonic and fluorescence signals, even when they are collected through the same detector without spectrally-specific filtering. Figure 4 shows the impetus for this idea. In the figure, the time until emission for SHG photons from corn starch granules and TPEF photons from 10 μm fluorescent microspheres (Invitrogen F8831) are measured using time-correlated single photon counting (TCSPC). (A different preparation of these same specimens is used in Figure 6). As expected, the harmonic signal arrives and decays essentially instantaneously, within the impulse response of the detection electronics. The fluorescence signal peaks at a measurable time delay with respect to the harmonic signal and displays a characteristic long-lived decay curve. Hence, through appropriate binning of the photon count as a function of time, we can discriminate between these two signals. Harmonic signals are only present immediately following the incident pulse, while fluorescent photons have a much longer-lived signal.

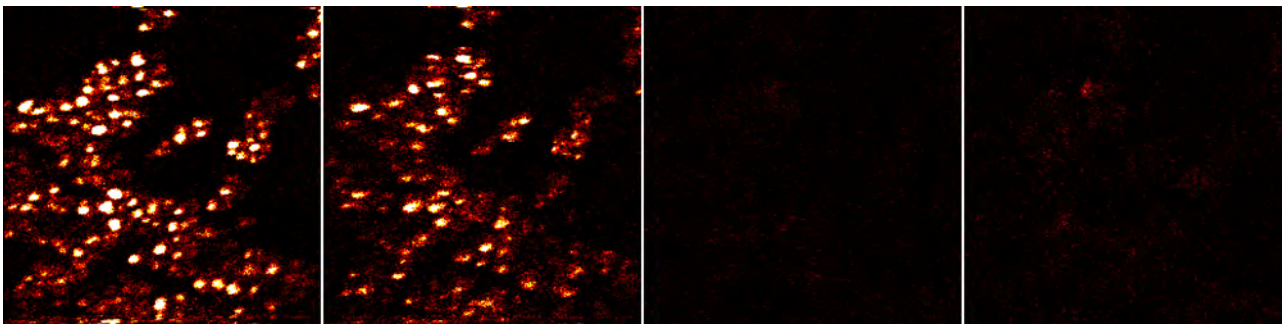

Figure 3 (online color at: www.biophotonics-journal.org) Simultaneous multi-depth SHG images of a sample of corn starch granules. Images were summed from a source data set composed of 900 frames of 256×1024 4-bit data collected at 30 Hz. Image depth increases from left to right by 7 μm. The field of view is 180 by 230 μm per image.

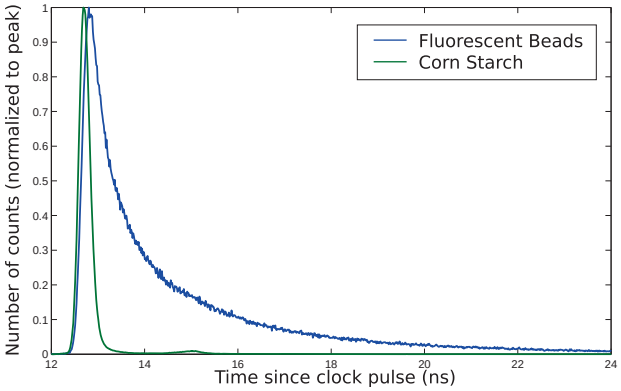

Figure 4 (online color at: www.biophotonics-journal.org) Time-correlated single photon counting traces for Invitrogen F8831 fluorescent microspheres (TPEF channel) and for corn starch granules (SHG channel).

The optical configuration for our single-element multimodal detection is the same as that discussed previously for our video-rate system. However, our field programmable gate array (FPGA) designs required a major upgrade in order to separate harmonic data from fluorescence data. For this work we utilized a bin size for the harmonic data of approximately 1.15 nanoseconds, corresponding to a delay through 6 gates of the Stratix III FPGA used by the DE3 board. Our previous designs relied on a clocking signal from the laser to enable a different beam-specific counter, depending on which beam is active at the time [12]. Separating out the harmonic data involved adding an internally delayed version of this timing signal to enable and disable an entirely separate set of counters meant specifically for the harmonic data (Figure 5).

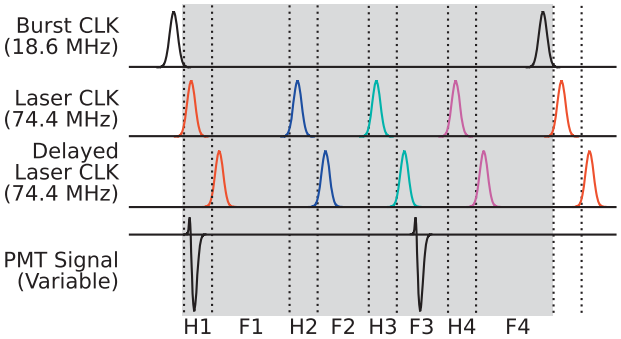

Figure 5 (online color at: www.biophotonics-journal.org) Timing of the FPGA counter bins indicating where photons detected by the photomultiplier tube (PMT) will be deposited. H1–H4 represent the harmonic bins for each of the four beams (~1.15 ns wide), and F1–F4 indicate the fluorescence bins (~5 ns wide). Since detection is operated in the photon-counting regime (variable detected events shown), a maximum of one photon is expected per bin.

3.2 Imaging results

By imaging a mixed sample containing both fluorescent microspheres and corn starch, we successfully demonstrated the ability of our photon counting electronics to differentiate between a harmonic response and a TPEF response. Figure 6a shows data collected with a 520 nm (SHG) interference filter in place to screen out the fluorescence channel, resulting in a 30% reduction in the signal of interest; Figure 6b displays data collected with a BG39 filter (for blocking only the excitation wavelength while allowing simultaneous transmission of the SHG and TPEF signals), exhibiting both the fluorescence and the SHG data; and Figure 6c shows a composite image of the data overlaying both channels of data from Figure 6b. This data is collected in the same manner as the video-rate data discussed previously, except that an additional harmonic channel is also returned (requiring a sustained data rate of 7.5 MiB/s).

4. Image deconvolution with multifocal systems

The ability to image multiple planes simultaneously lends itself to the idea that methods developed for wide-field imaging for improving spatial content may now also be viable for the mulitfocal multiphoton laser scanning microscope (MPLSM) geometries described here. Structured illumination microscopy (SIM), sometimes referred to as patterned illumination microscopy, is one such method [18–24]. SIM microscopy exploits spatial frequency mixing to downshift undetectable spatial frequencies into the passband of a wide-field microscope. This task is accomplished by projecting illumination patterns onto the specimen and detecting the down-shifted high spatial frequency components that are filtered by the objective lens. By appropriate data collection and reconstruction, the region of frequency space that is "visible" to a microscope may be increased, thereby improving the spatial resolution of the imaging apparatus. Moreover, by exploiting nonlinearities in photoresponse, the resolution enhancement attainable is limited only by experimental parameters, such as the signal-to-noise ratio (SNR) [20].

Despite the impressive spatial resolution attainable with wide-field SIM (WFSIM), the nature of wide-field imaging limits the applicability of the technique in highly scattering media. Since imaging is done via spatial registration with a CCD camera, is very susceptible to image quality degradation from the scattering of signal photons. When a signal photon is scattered, it may be detected at a pixel other than the one conjugate to its location in the specimen

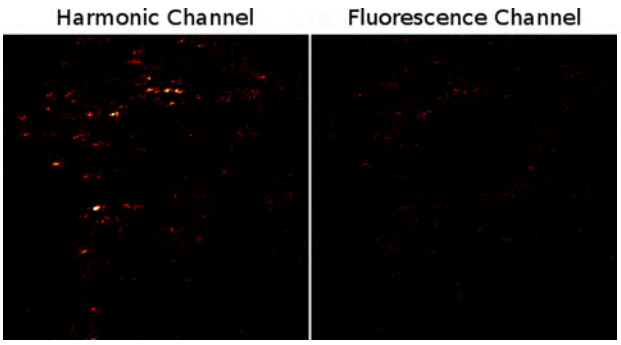

a) Fluorescent beads and corn starch with 520 nm interference filter. Note that the reduction in counts as compared to (b) is a result of the 30% transmission of the filter.

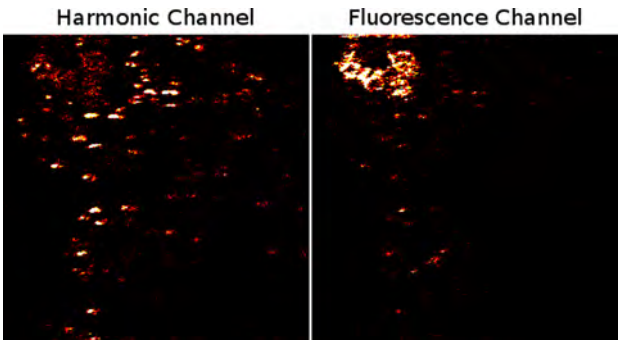

b) Fluorescent beads and corn starch with BG39 filter.

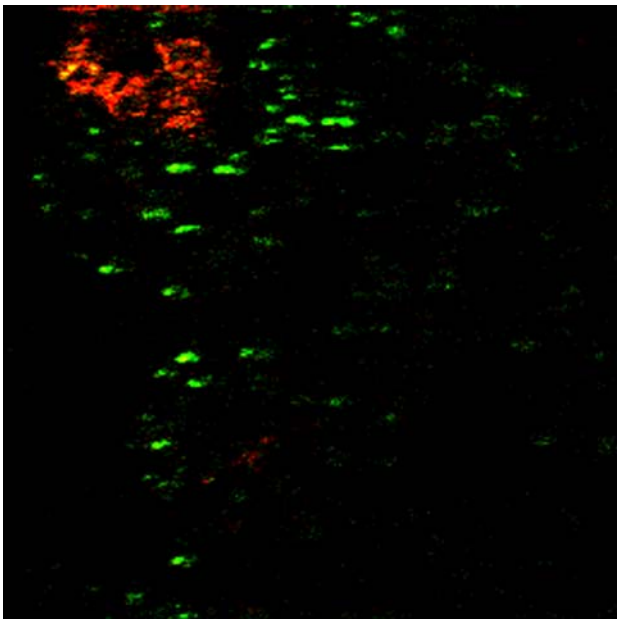

c) False color overlapped image of fluorescent beads (orange) and corn starch (green) imaged with a BG39 filter.

Figure 6 (online color at: www.biophotonics-journal.org) Images of a sample of fluorescent beads mixed with corn starch granules. Images were summed from a source data set composed of 900 frames of 512×1024 4-bit data collected at 30 Hz and are from one representative beam of the data (a 256×512 region, corresponding to two channels representing 180 by 230 μm). (**a**) and (**b**) show the second harmonic channel on the left and the TPEF channel on the right, and (**c**) shows these two channels overlapped in a false color image.

plane, resulting in significant blurring of the image [8, 25]. The upshot of this effect is that highly scattering specimens, such as biological tissues, are restricted to thin preparations (~10 μm; [26]) to avoid image blurring that would offset the resolution enhancement.

As we have already seen, the photon counting modality allows one to use whole-field detection with multiple focal spots to eliminate the scattering ambiguity. To date, however, no implementation of SIM has been demonstrated with the whole-field detection inherent to MPLSM, although it has been suggested theoretically [27]. In this section, we present multiphoton laser-scanning structured illumination microscopy (MPLS-SIM) as a method for efficient image deconvolution. Ultimately, this work suggests that MPLS-SIM may be a viable technique for achieving spatial resolution beyond that defined by the diffraction limit of light in far-field multiphoton microscopy with whole-field detection. An advantage of this technique, used in conjunction with a multifocal system, is its ability to collect many images simultaneously, thereby allowing for MPSIM images to be collected in a significantly more efficient manner.

4.1 Experimental Setup

Two pulse trains from our six-beam $Yb:KGd(WO_4)_2$ laser oscillator [11], with a central wavelength of 1038 nm and pulse width of 200 fs, was used as the excitation source for a the MPLSM setup [28]. The two pulse trains are spatially separated with pulses tempo-

rally delayed by 6 ns repeating at an oscillator frequency of 18.6 MHz. Using our previously developed custom-built electronics [29], we are able to rapidly demultiplex a photon-counted pulse train from a single photomultiplier tube (PMT) to obtain two images in a single scan of the field of view (FOV). A polarizing beam splitter (PBS) and $\lambda/2$ waveplate were used to combine the two beams with orthogonal polarization states into a single 37.2 MHz pulse train.

Gratings were projected onto the specimen plane by modulating the polarization state of each excitation beam with a 512×512-pixel nematic liquid-crystal spatial light modulator (LC-SLM; Boulder Nonlinear Systems). The pulse trains were focused onto the face of the LC-SLM, which was, in turn, image relayed to the focal plane of the excitation objective (Figure 7). Since the birefringence of the LC-SLM depends upon the voltage applied to each pixel, this device may be thought of as an array of tiny programmable waveplates, allowing for accurate control of the polarization state of each pulse train in the specimen plane. Sinusoidal patterns were applied to the LC-SLM with a custom MATLAB® GUI (written in house), which oscillate between S and P polarization states. By rejecting one polarization state with a PBS, we are able to modulate the excitation intensity as a function of scan position within the specimen plane. This system allows for full programmable control of the grating frequency $\boldsymbol{k}_g$ in the imaging plane.

An example of dual gratings taken simultaneously is shown in Figure 8. The gratings are visualized by projecting them onto an aqueous specimen of Rhodamine-6G in water and utilizing the multifocal demultiplexing techniques described above to form two images of the epi TPEF signal. Each image displayed in Figure 8 is a merged image of the response from the orthogonal polarization states. While the phase shift between the gratings in each image is 180 degrees, the utility of the demultiplexing technique for fast image acquisition in highly scattering media is clear: by appropriate tailoring of the input polarization state of multiple beams, all images needed for SIM at a single angle can be collected simultaneously.

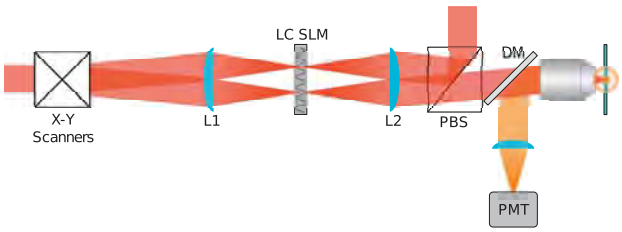

Figure 7 (online color at: www.biophotonics-journal.org) Experimental configuration for a multibeam MPLS-SIM system. An LC-SLM is imaged to the specimen plane of the microscope, where the voltage applied to the device modulates the polarization state of the excitation source. A polarizing beam splitter (PBS) is used to reject one polarization state, thereby projecting a grating onto the specimen plane. The nonlinear signal is collected in a whole-field scheme. While only a single beam at differing scan angles is shown for clarity, in practice the single beam is two spatially overlapped pulse trains to achieve multifocal imaging. All images in this section were taken with a 0.75 NA objective.

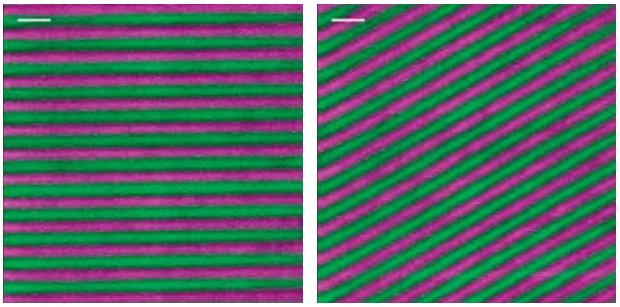

Figure 8 (online color at: www.biophotonics-journal.org) Simultaneously projected gratings at differing angles. Each image is a composite of two images collected simultaneously with orthogonal polarization states. The result is two gratings that are out of phase with one another. Here the images were collected by imaging the TPEF signal from a bath of Rhodamine-6G. Scale bars are 5 μm.

4.2 Example image deconvolution: Tag-RFP labelled crystalline cellulose fibers

An example of the utility of image deconvolution with multiple gratings is shown in Figure 9, which shows the second harmonic generation (SHG) signal collected in the epi direction from crystalline cellulose fibers labeled with a monomeric red fluorescent protein (mRFP). The image on the lower left is the summation of images collected with 6 grating directions and 7 phase shifts using the MPLS-SIM technique, while the image on the upper left was reconstructed with the deconvolution method. Data collection and image reconstruction were based on methods previously described by Gustafsson and coworkers [18, 20, 30]. A custom LabVIEW™ program that controls the imaging setup (written in house) was interfaced with the MATLAB® GUI for automated data collection for a given number of angles and phase shifts. The number of phase shifts was determined prior to data collection by projecting gratings on aqueous samples of Rhodamine-6G in water and counting the number of peaks that could be seen in reciprocal space.

From Figure 9, it is evident that the spatial resolution in the MPLS-SIM image is improved. As indicated in previous reports [27], this result is due

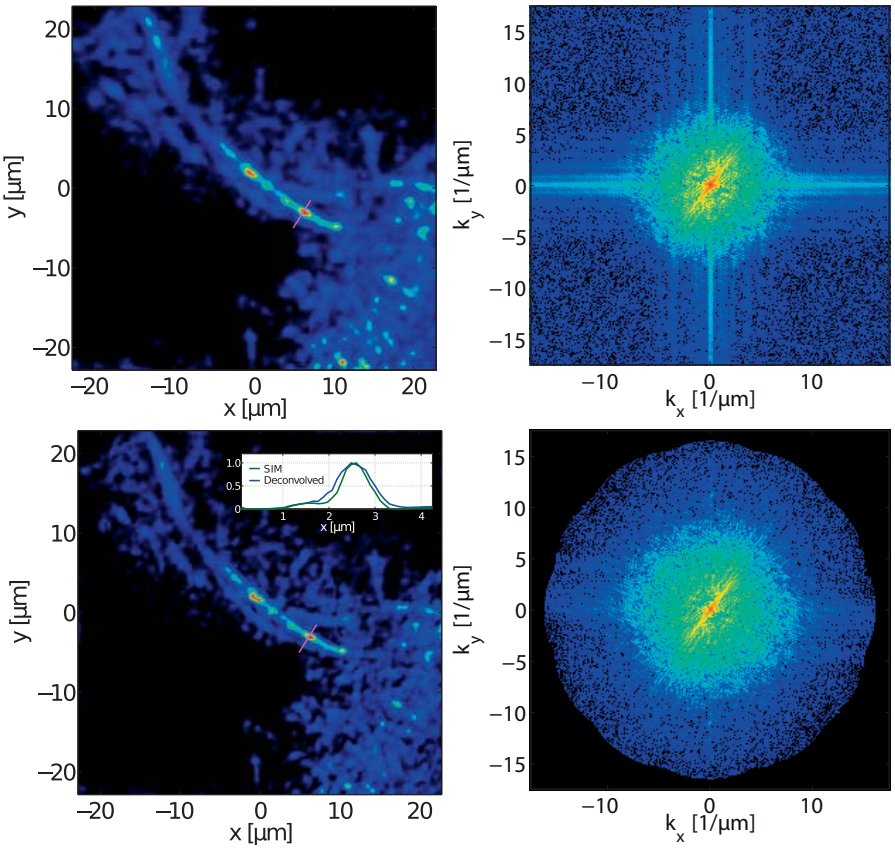

Figure 9 (online color at: www.biophotonics-journal.org) Image deconvolution in second harmonic generation imaging of crystalline cellulose fibers. The top images represent the conventional multiphoton image, formed by summation of all images with projected gratings, while the lower row displays the deconvolved MPLS-SIM image. Images on the left are in image space, while the Fourier domain for each image is displayed in the right column. It is clear that in Fourier space, the MPLS-SIM image contains additional information components that lie beyond the passband of our multiphoton microscope. A lineout demonstrating this improvement is shown as an inset to the lower left image.

to the slight increase in content at higher spatial frequencies. The additional information can be seen in the right column of Figure 9, where the spatial frequencies within the deconvolved image are shown on a logarithmic scale. As compared to the reciprocal space of the conventional image, there is a notable information gain at higher spatial frequencies.

4.3 Challenges in pushing MPLS-SIM image reconstruction forward

While there is a gain in the spatial resolution in the SHG images shown in Figure 9, resolution enhancement in TPEF from the mRFP, which was collected simultaneously, did not show significant improvement. Instead, we find several artifacts to the image reconstruction process that result from spurious high-frequency components in reciprocal space (data not shown). The result is ringing at high frequencies in real space that significantly negatively impact the spatial resolution of the image. This ringing appears to be related to photobleaching in the image collection process. When the first grating is projected onto the specimen, the fluorophores within the sample plane are selectively photobleached along the grating maxima. This changes the density of fluorophores available for imaging in subsequent images. Therefore, each successive image taken with a projected grating contains frequency mixing between the specimen and the gratings that were projected previously. Effectively, this process can be viewed as taking an image of a different specimen on each phase shifted image, thereby resulting in significant cross-talk between information components in reciprocal space, resulting in high-frequency components in the reconstructed image.

5. Single element detection using a line cursor excitation source

As stated in the introduction, the first real-time multiphoton imaging system incorporated a line cursor geometry [1]. This system used a 100 kHz repetition rate chirped pulse amplification $Ti:Al_2O_3$ laser system as the excitation source and utilized a two-dimensional detector. Here we demonstrate that it is possible, through spatial modulation of the beam, to make the line cursor excitation compatible with single element detection, and that imaging can be done using a $Ti:Al_2O_3$ oscillator system. While these results are preliminary, they point the way to a new paradigm for rapid volumetric multiphoton imaging

that will ultimately prove straight-forward for the biological community to implement.

The schematic for this system is shown in Figure 10. The Ti : Al_2O_3 oscillator is an extended cavity system operating at 23 MHz and 800 nm with a pulse duration of 70 fs and pulse energies up to 20 nJ. This pulse energy and repetition rate are a good combination for use with line cursor geometries to ensure sufficient peak intensity across the line focus for multiphoton excitation. The output of the laser is up-collimated to 10 mm, and the line cursor is created at an intermediate plane by a 10 mm focal length cylindrical lens. A modulator placed at the focal plane of the cylindrical lens produces an intensity modulation with a frequency that sweeps linearly across the line focus. The modulator uses a transmission pattern shown in Figure 12 that, when spun at constant angular velocity of 100 Hz, produces modulation frequencies centered at 18 kHz with a width of several kilohertz. The chirped intensity modulation imposes modulation frequencies that are lower near the inner disk radius, and higher modulation frequencies on the edge of the disk. The spatial variation in modulation frequency causes sequential points to be modulated at slightly higher frequencies as a function of spatial position [31]. In this manner spatial location is selectively encoded as modulation frequency. This encoding allows line spatial information to be extracted from the electronic signal spectrum acquired from a single element detector, such as a photodiode or PMT. As the modulation imposed on the excitation pulse train is at a frequency much slower than fluorescent decay rates, the fluorescent yield adiabatically follows the modulated excitation. Hence, the spatially-chirped intensity modulation of the excitation beam is transfered to the fluorescence emission. Collection of the fluorescent emission in either transmitted or epi configurations on a single element detector allows for recovery of the fluorophore concentration across the modulated line cursor. The line image is recovered through a straightforward Fourier transform of the time-varying detected signal – be it from TPEF or the fundamental excitation beam itself.

After the mask, the beam is directed through a single-axis scanner, and relayed to the specimen plane. The excitation optic is a 0.75 NA objective. The TPEF signal is collected in the epi direction by a PMT, and the fundamental is collected in transmission by a Si photodiode. The scan time is adjusted as appropriate for the signal levels coming from the specimen. In this case our multimodal detection is a nonlinear signal (TPEF) and a linear signal (the light from the excitation beam).

Figure 12 shows images obtained with the system, and Figure 11 shows the mask used to modulate the beam. The specimen shown in the left image series of Figure 12 was a simple wire test grid immersed in Rhodamine-6G. The upper left image is the TPEF signal, and the lower left image is created with the transmitted signal from the laser beam. The right image shown in Figure 12 is a TPEF image of an onion layer dyed with Rhodamine-6G. The nucleus and cell walls can be resolved. The lateral image resolution for the system is 10 μm, which is substantially below the diffraction-limited resolution of the 0.75 NA objective (~0.65 m). In these images, the resolution is limited by the mask. For this demonstration, the pattern shown in Figure 11 was printed on a simple CD and only consists of low spatial frequencies. The time varying diffraction pattern, created by rotating the mask, results in substantially underfilling the objective, and hence severely limits the image resolution (and hence the number of pixels within the image). This is in no way a fundamental limitation. We are presently fabricating new masks that will result in a time-varying diffraction pattern that will completely fill the objective and produce images that are limited in resolution by the excitation objective NA. Finally,

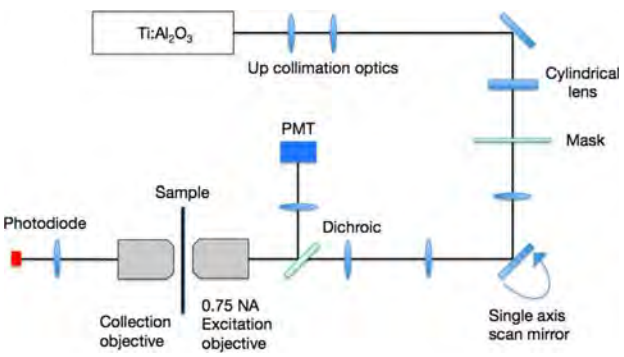

Figure 10 (online color at: www.biophotonics-journal.org) Spatially modulated, line cursor excitation multiphoton microscope schematic. The excitation course is an extended cavity Ti : Al_2O_3 oscillator operating at 23 MHz.

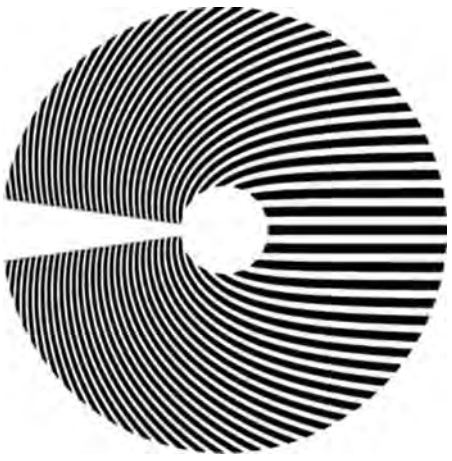

Figure 11 Mask pattern which is used to create the spatially chirped intensity modulation on the excitation beam.

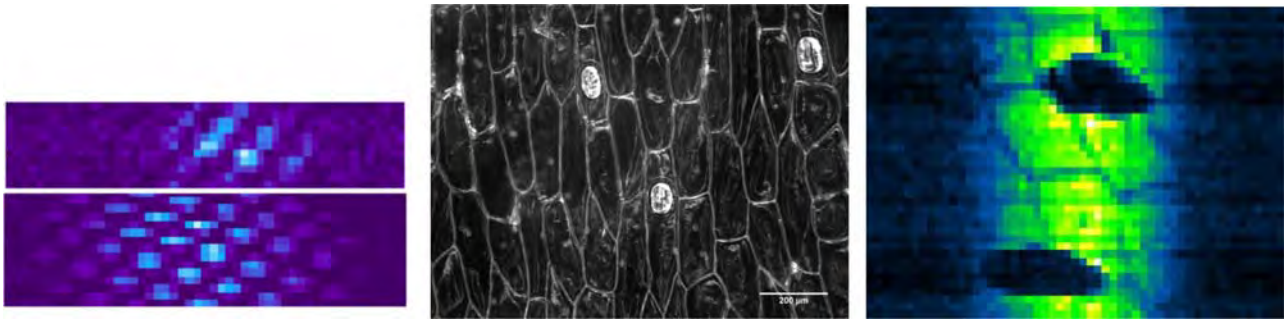

Figure 12 (online color at: www.biophotonics-journal.org) Upper left: TPEF image of test grid. Lower left: image of test grid created from fundamental beam. For scaling, the center to center spacing of adjacent squares in each of the images is 75 μm. Center: dark field image of an onion skin. The central portion of this sample was used to create the TPEF image. Right: TPEF image of the onion skin. The dark field image was taken with a separate microscope, resulting in the different sample orientation and magnification apparent in the images. Approximately 9 nJ per pulse, as measured in front of the microscope, was used to create the TPEF images.

the non-uniformity in intensity of the line cursor is also evident in the images – especially so in the TPEF image given its nonlinear dependence. This is due to the nature of the Gaussian beam and can ultimately be accounted for in post image processing – only raw data is shown here.

6. Conclusion

Multifocal imaging is an effective way of increasing the imaging throughput of multiphoton microscopes. By shifting the detection to a photon-counting mode, the scattering ambiguity that accompanied the multifocal approach can be entirely eliminated as single-element detection becomes compatible with a multibeam imaging system. In this paper we have extended the photon-counting capability and data transfer rates significantly. Specifically, the data rates have been increased by a factor of 20 and the pixel dwell time reduced by a factor of 50. The result is a new technology that enables multiphoton microscopes to capture entire image volumes dynamically. Multiple focal planes are captured in parallel using a non-perturbative volumetric scanning process of the specimen.

As the data rates have increased, the potential has emerged for novel detection methods. For instance, it is extremely interesting to have the capability to detect mulitple modalities simultaneously, such as second harmonic generation and TPEF. To date, detection of these signals has required the implementation of two separate detectors, multiple filters and dichroics. We have shown that two such signals can be detected with a single detector without the use of a frequency selective filter. While there is cross talk in this implementation, it appears that there is sufficient selectivity to effectively discriminate between the two signals.

With the ability to rapidly accumulate images from multiple foci, it becomes interesting to explore methods that would enable accurate image deconvolution throughout the specimen volume. Here we have examined one method which involves writing gratings through the use of a programmable spatial light modulator. The multifocal approach makes it possible to write structured patterns at multiple angles and at multiple depths simultaneously, illustrating one possible method of rapid specimen volume characterization that could improve our ability to more accurately extract spatial information.

Finally, we have begun exploring new methods for extending the excitation source geometry that could lead to further simplification in a microscope designed for rapid volume characterization. We have shown that multimodal detection is possible using line cursor excitation sources that are spatially modulated. Importantly, this implementation retains single-element detection capability and has the potential of high-speed volume imaging without the need for specialized laser sources. This technology should, therefore, be quite straightforward to implement into existing multiphoton imaging systems with minimal modification.

Acknowledgments We would like to acknowledge support from the National Renewable Energy Laboratory CRADA program. This work was funded by the National Institute of Biomedical Imaging and Bioengineering under the Bioengineering Research Partnership EB-003832 and the National Science Foundation under DBI-0852868. Eric V. Chandler acknowledges the support of the Renewable Energy Materials Research Science and Engineering Center under Grant No. DMR-0820518. Shi-You Ding acknowledges the support of the US Department of Energy, the Office of Science, Office of Biological and Environmental Research, the BioEnergy Science Center (BESC), a DOE Bioenergy Research Center. Jing. W. Wang acknowledges support from the National Institute of Health under NIH/NIDCD (5R01DC009597).

Erich E. Hoover received the B.Sc. degree in engineering physics, in 2007, and the M.Sc. degree in engineering with an electrical specialty, in 2008, from the Colorado School of Mines, Golden, where he is currently working toward a Ph.D. degree in applied physics. He was a Computer Programmer and Software Engineer at dBm Optics, Inc. for seven years. His current research interests include applying photon counting techniques toward simultaneous imaging of multiple depths inside scattering media.

Jeffrey J. Field received the B.Sc. and M.Sc. degrees in engineering physics in 2005 and 2006, respectively, and the Ph.D. degree in applied physics, in 2010, all from the Colorado School of Mines. He is currently a Postdoctoral Fellow in the Department of Electrical and Computer Engineering at Colorado State University. Dr. Field is a member of the Optical Society of America and the Society of Photo-Optical Instrumentation Engineers.

David G. Winters received his undergraduate degree in physics from the University of Washington in 2005. He then began graduate work at Colorado State University in electrical engineering with a focus in optics. He completed his Master's degree in 2007 and is currently pursuing his Ph.D. with research interests in novel Raman and nonlinear microscopy techniques.

Michael D. Young received the B.Sc. degree in engineering physics, in 2008, from the Colorado School of Mines, Golden, where he is currently working toward the Ph.D. degree. His research interests include simulated optical design, laser microscopy, and physics pedagogy.

Eric V. Chandler is a graduate research assistant in the Renewable Energy Materials Research Science and Engineering Center at the Colorado School of Mines. His current research centers on the non-linear optical characterization of nanostructured materials for photovoltaic applications, with a specific focus on individual nanocrystallites.

John C. Speirs is a graduate student at the Colorado School of Mines in applied physics. He received his B.Sc. degree in engineering physics from the same school. He has participated in research in objective design and novel multiphoton microscopy techniques.

Jacob T. Lapenna received his A.O.S. degree from Universal Technical Institute, with a focus in automotive and diesel technologies, in 2005. He worked for Audi as a technical specialist until 2007. He then went on to receive his B.Sc. degree in engineering physics from the Colorado School of Mines in 2011. He is currently working on his Ph.D. in electrical engineering at Princeton University. His thesis focuses in nonlinear optics with an emphasis on the advancement of novel imaging techniques.

Susy M. Kim is currently a post-doctoral fellow in Jing Wang's group at the University of California, San Diego. She received her Ph.D. in Neuroscience from the University of Arizona in 2007. She is currently investigating how odor information is integrated and used to influence behavior in the fruit fly.

Shi-you Ding is a plant biologist and enzyme biochemist specializing in the ultrastructure of plant cell walls and their degrading systems. He has pioneered nanometer-scale studies of plant cell wall structures and the changes occurring in them during biomass conversion processes. He initiated the development of the Biomass Surface Characterization Laboratory (BSCL) at NREL, which enables chemical and spatial characterization of biodegrading systems at the nanometer scale. Dr. Ding also has discovered new multienzyme cellulosomes and thermal tolerant cellulases.

Randy A. Bartels is a Monfort Professor in the Departments of Electrical and Computer Engineering, Chemistry, and Biomedical Engineering at Colorado State University, Fort Collins. His interests include developing techniques for nonlinear optical spectroscopy and microscopy. He has received numerous awards, including the Adolph Lomb Medal, an NSF CAREER, a Beckman Young Investigator Award, a Photonics Society Young Investigator Award, and a PECASE. He is a Fellow of the Optical Society of America.

Jing W. Wang is an Associate Professor in the Section of Neurobiology at the University of California, San Diego. He investigates neural circuits underlying olfactory based behaviors in the fruit fly. He received his Ph.D. in Neurobiology from the University of Iowa in 1997 in the laboratory of Chun Fan Wu, pursued postdoctoral studies at Bell Labs/Lucent Technologies with Alan Gelperin and Columbia University with Richard Axel, and is a Beckman Young Investigator and Searle Scholar.

Jeff A. Squier received the B.Sc. degree in engineering physics, and the M.Sc. degree in applied physics from the Colorado School of Mines, Golden, and the Ph.D. degree in optics, in 1992, from the University of Rochester, Rochester, NY. He was a Research Faculty at the Center for Ultrafast Optical Science, University of Michigan, and in 1995, joined the University of California, San Diego. Since 2002 he has been with the Department of Physics, Colorado School of Mines, Golden.

References

[1] G. J. Brakenhoff, J. Squier, T. Norris, A. C. Bliton, M. H. Wade, and B. Athey, J. Microsc. **181**, 253–259 (1996).

[2] J. Bewersdorf, R. Pick, and S. W. Hell, Opt. Lett. **23**, 655–657 (1998).
[3] M. Straub and S. W. Hell, Bioimaging **6**, 177–185 (1998).
[4] A. H. Buist, M. Müller, J. Squier, and G. J. Brakenhoff, J. Microsc. (Oxford) **192**, 217–226 (1998).
[5] A. Egner and S. W. Hell, J. Opt. Soc. Am. A **17**, 1192–1201 (2000).
[6] V. Andresen, A. Egner, and S. W. Hell, Opt. Lett. **26**, 75–77 (2001).
[7] K. Bahlmann, P. T. So, M. Kirber, R. Reich, B. Kosicki, W. McGonagle, and K. Bellve, Opt. Express **15**, 10991–10998 (2007).
[8] K. H. Kim, C. Buehler, K. Bahlmann, T. Ragan, W.-C. A. Lee, E. Nedivi, E. L. Heffer, S. Fantini, and P. T. C. So, Opt. Exp. **15**, 11658–11678 (2007).
[9] J. Martini, V. Andresen, and D. Anselmetti, J. Biomed. Opt. **12**, 034010 (2007).
[10] A. Cheng, J. T. Goncalves, P. Golshani, K. Arisaka, and C. Portera-Cailliau, Nat. Methods **8**, 139–142 (2011).
[11] K. E. Sheetz, E. E. Hoover, R. Carriles, D. Kleinfeld, and J. A. Squier, Opt. Exp. **16**, 17574–17584 (2008).
[12] E. E. Hoover, M. D. Young, E. V. Chandler, A. Luo, J. J. Field, K. E. Sheetz, A. W. Sylvester, and J. A. Squier, Opt. Express **2**, 113–122 (2010).
[13] E. J. Botcherby, R. Juskaitis, M. J. Booth, and T. Wilson, Opt. Lett. **32**, 2007–2009 (2007).
[14] R. Carriles, K. E. Sheetz, E. E. Hoover, J. A. Squier, and V. Barzda, Opt. Exp. **16**, 10364–10371 (2008).
[15] I. Veilleux, J. Spencer, D. Biss, D. Côté, and C. Lin, IEEE J. Sel. Top. Quantum Electron. **14**, 10–18 (2008).
[16] A. Edelstein, N. Amodaj, K. Hoover, R. Vale, and N. Stuurman, Curr. Protoc. Mol. Biol., 14.20.1–14.20.17 (2010).
[17] J. D. Driscoll, A. Y. Shih, J. J. Field, G. A. White, J. A. Squier, G. Cauwenberghs, and D. Kleinfeld, J. Neurophysiol. **105**, 3106–3113 (2011).
[18] M. Gustafsson, J. Microscopy **198**, 82–87 (2000).
[19] R. Heintzmann, Micron **34**, 283–291 (2003).
[20] M. Gustafsson, Proc. Nat. Acad. Sci. **102**, 13081–13086 (2005).
[21] R. Heintzmann and G. Ficz, Briefings Funct. Genomics. **5**, 289 (2006).
[22] R. Heintzmann, T. Jovin, and C. Cremer, J. Opt. Soc. Am. A **19**, 1599–1609 (2002).
[23] R. Heintzmann and P. Benedetti, Appl. Opt. **45**, 5037–5045 (2006).
[24] R. Heintzmann and M. G. L. Gustafsson, Nat. Photonics **3**, 362–364 (2009).
[25] F. Helmchen and W. Denk, Nat. Methods **2**, 932–940 (2005).
[26] V. Ntziachristos, Nat. Methods **7**, 603–614 (2010).
[27] J. Lu, W. Min, J. Conchello, X. Xie, and J. Lichtman, Nano. Lett. **9**, 3883–3889 (2009).
[28] J. J. Field, K. E. Sheetz, E. V. Chandler, E. E. Hoover, M. D. Young, S. you Ding, A. W. Sylvester, D. Kleinfeld, and J. A. Squier, IEEE J. Sel. Top. Quant. Elec. **99**, 1–15 (2011).
[29] E. Chandler, E. Hoover, J. Field, K. Sheetz, W. Amir, R. Carriles, S. Ding, and J. Squier, App. Opt. **48**, 2067–2077 (2009).
[30] M. Gustafsson, L. Shao, P. Carlton, C. Wang, I. Golubovskaya, W. Cande, D. Agard, and J. Sedat, Biophys. J. **94**, 4957–4970 (2008).
[31] G. Futia, P. Schlup, D. G. Winters, and R. A. Bartels, Opt. Express **19**, 1626–1640 (2011).

